Nonlinear enhancement of measurement precision via a hybrid quantum switch

Lei Chen,[1,2,3] Yuxiang Yang,[4] Gong-Chu Li,[1,2,3,5] Xu-Song Hong,[1,2,3,5] Si-Qi Zhang,[1,2,3]
Hua-Qing Xu,[1,2,3] Yuan-Cheng Liu,[1,2,3] Giulio Chiribella,[4,6,7,*] Zhibo Hou,[1,2,3,5]
Geng Chen,[1,2,3,5,†] Chuan-Feng Li,[1,2,3,5,‡] and Guang-Can Guo[1,2,3,5]

[1]*Laboratory of Quantum Information, University of Science and Technology of China, Hefei 230026, People's Republic of China*
[2]*CAS Center For Excellence in Quantum Information and Quantum Physics, University of Science and Technology of China, Hefei, Anhui 230026, China*
[3]*Anhui Province Key Laboratory of Quantum Network, Hefei, Anhui 230026, China*
[4]*QICI Quantum Information and Computation Initiative, Department of Computer Science, The University of Hong Kong, Pokfulam Road, Hong Kong 999077, China*
[5]*Hefei National Laboratory, University of Science and Technology of China, Hefei, China*
[6]*Department of Computer Science, University of Oxford, Parks Road, Oxford OX1 3QD, United Kingdom*
[7]*Perimeter Institute for Theoretical Physics, Caroline Street, Waterloo, Ontario N2L 2Y5, Canada*

(Received 24 December 2025; revised 15 June 2026; accepted 29 June 2026; published 5 August 2026)

Quantum metrology promises measurement precision beyond the classical limit by using suitably tailored quantum states and detection strategies. However, scaling up this advantage is experimentally challenging, due to the difficulty of generating high-quality large-scale probes. Here, we build a photonic setup that achieves enhanced precision scaling by manipulating the probe's dynamics through operations performed in a coherently controlled order. Our setup applies an unknown rotation and a known orbital angular momentum increase in a coherently controlled order, in a way that reproduces a hybrid quantum switch involving gates generated by both discrete and continuous variables. The unknown rotation angle θ is measured with precision scaling as $1/4\,ml$ when a photon undergoes a rotation of $2m\theta$ and an angular momentum shift of $2l\hbar$. With a practical enhancement factor as high as 2317, we achieve a normalized precision of approximately equal to 10^{-4} rad per photon. The precision enhancement consumes only a linearly increasing number of applications of the gates while achieving a nonlinear scaling of the precision. We further indicate that this nonlinear enhancement roots in an in-depth exploration of the Heisenberg uncertainty principle (HUP). The very quantum noncommutativity that imposes fundamental limitations on measurement precision under the HUP is transformed into a valuable quantum resource that enables the observed nonlinear enhancement.

DOI: 10.1103/d5bb-5vmv

I. INTRODUCTION

Precision measurements normally consist of three steps: preparation of the probe state, encoding of the target parameter, and detection. Standard methods using N unentangled probe particles can reduce the measurement uncertainty to $\Delta \propto 1/\sqrt{N}$, corresponding to the central limit scaling of classical statistics [1,2]. Quantum metrology offers an opportunity to boost the precision beyond the classical limit, for example, by initializing the probe particles into suitably designed quantum states, such as NOON states [3–5] or squeezed states [6]. With such quantum resources as the probe, the precision can surpass the classical limit or even attain the Heisenberg limit $\Delta \propto 1/N$ [7]. To date, however, preparing large-scale quantum entangled states [8,9] is still a daunting task, and hence the $1/N$ scaling can only survive for relatively small values of N. The squeezing-enhanced precision is feasible within the scope of current technological capabilities. However, the enhancement factor is constrained and highly susceptible to noise, such as photon loss [10]. Although it has been shown that the Heisenberg limit could persist for large N in some special measurement scenarios [11,12], a simple way to scale up quantum metrology advantages is currently missing.

Recently, research in the foundations of quantum mechanics identified a new quantum resource, namely, the ability to perform operations in an indefinite causal order (ICO) [13–15], which utilizes a quantum system to control the order of the gates and arrives at quantum processes in which the constituent events do not have a definite causal structure [14–16]. A particular form of

*Contact author: giulio@cs.hku.hk
†Contact author: chengeng@ustc.edu.cn
‡Contact author: cfli@ustc.edu.cn

ICO, known as the quantum switch (QS) [15], provides coherent control over the order of operations and has been found to have applications in various areas of quantum information [17–28], including quantum metrology [29–32]. In particular, the quantum switch was shown to offer a quadratic scaling advantage in the measurement of a geometric phase associated with two groups of N phase-space displacements [29,32]. Notably, this quadratic scaling via ICO does not violate the Heisenberg uncertainty principle, because the variances of the generators are improved. Thus, without breaking any fundamental rule, the resources arising from the ICO lead to a leap in measurement precision.

Although ICO offers intriguing advantages in quantum metrology, these advantages have been so far limited to rather specific problems. Notably, no application has been found for practically relevant problems such as phase estimation or, more generally, the estimation of a single parameter associated with quantum dynamics. Exploiting ICO in the single-parameter scenario appears far from straightforward, especially in the ideal case of unitary dynamics with time-dependent Hamiltonians, because the unitary evolution commutes at all times, and therefore the order in which different snapshots of dynamical evolution are executed does not affect the final state of the probe. A possible way around this is to combine the probed dynamics with some known operations and to combine these operations in an ICO. While these additional operations can always be regarded as part of the setup, the use of ICO between known operations and unknown dynamics can offer practical benefits, such as enabling nonclassical precision scalings with easy-to-prepare probe states.

In this work, we demonstrate a practical application of ICO in estimating an unknown rotation angle by introducing coherently controlled orders of two noncommutative gates, namely, the gates that, respectively, generate displacements in orbital angular momentum (OAM) and the azimuth angle. A hybrid setup inspired by the quantum switch is built to probe a rotation angle θ imparted by a rotating gate on an arbitrary optical wavefront. By combining m such rotating gates with additional gates that each alter the OAM by $l\hbar$ into an ICO configuration, we achieve a precision enhancement in the estimation of θ by a factor of $4ml$, which we experimentally demonstrate up to the value 4096 by setting $l = 128$ and $m = 8$. By taking noise into account, the overall enhancement can maintain a high factor of 2317, and the ultimate precision in our experiment is $0.0105''$ when using 7.16×10^7 photons, corresponding to a normalized precision of 4.3×10^{-4} rad for one photon.

II. RESULTS

Here, we provide a setup for the estimation of an unknown rotation angle θ imprinted on the OAM degrees of freedom. These degrees of freedom are characterized by two quantum-mechanical observables, namely, the azimuth angle $\hat{\theta}$ and the z component of the orbital angular momentum $\hat{L}_z$. The commutation between $\hat{\theta}$ and $\hat{L}_z$ manifests a complex expression due to the imposition of periodic boundary conditions [33,34]. For simplicity and consistency with our experimental setting, we constrain the rotation angle as $\theta \in (-\pi, \pi)$. Consequently, the two observables adhere to the canonical commutation relation $[\hat{\theta}, \hat{L}_z] = i\hbar$, which parallels the commutation relation between position and momentum. A significant difference here is that the spectrum of the orbital angular momentum is discrete. Physically, the OAM is not a continuous degree of freedom because only the Laguerre-Gaussian beam with an integer topological charge is the eigenmode of propagation. Thanks to the discreteness of the angular momentum, $\hat{L}_z$ not only functions as the noncommutative observable of $\hat{\theta}$ but also provides a well-defined degree of freedom that enables precise implementation of the displacement. This situation is different from the case of continuous observables, like position and momentum, for which precise control of displacements is more challenging.

Our setup probes an unknown rotation $D_{2m\theta} = e^{-\frac{2i}{\hbar} m \hat{L}_z \theta}$ by sandwiching it between the discrete operations $D_{l\hbar} = e^{il\hat{\theta}}$ and $D_{l\hbar}^{\dagger}$, which shifts the z-component angular momentum upward and downward, respectively, by $l\hbar$. The order of the two shifts is coherently controlled by a qubit, as illustrated in Fig. 1, giving rise to the overall evolution $W \coloneqq D_{l\hbar}^{\dagger} D_{2m\theta} D_{l\hbar} \otimes |0\rangle\langle 0| + D_{l\hbar} D_{2m\theta} D_{l\hbar}^{\dagger} \otimes |1\rangle\langle 1|$. The operator W is unitarily equivalent to the operator

$$W_{\mathrm{QS}} = D_{2m\theta} D_{2l\hbar} \otimes |0\rangle\langle 0| + D_{2l\hbar} D_{2m\theta} \otimes |1\rangle\langle 1|, \quad (1)$$

which reproduces the same evolution that would arise if the gates $D_{2m\theta}$ and $D_{2l\hbar}$ were combined in the quantum switch. With a little abuse of terminology, in the following,

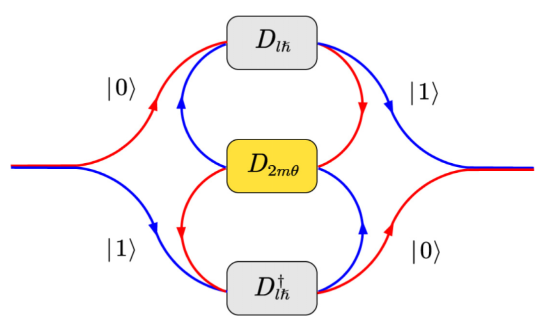

FIG. 1. Quantum switch setup for the measurement of the rotation angle. A rotation of the orbital angular momentum, denoted by $D_{2m\theta}$, is performed between an operation $D_{l\hbar}$ that increases the orbital angular momentum and its inversion $D_{l\hbar}^{\dagger}$, with the order of these two operations coherently controlled by the state of a qubit.

we will refer to our setup as a hybrid quantum switch setup, the term "hybrid" referring to the presence of both discrete and continuous variables.

Since the observables $\hat{\theta}$ and $\hat{L}_z$ are canonically conjugate, the corresponding displacement satisfies the relation $D_{2l\hbar}D_{2m\theta} = e^{i4ml\theta}D_{2m\theta}D_{2l\hbar}$, which implies $W_{\rm QS} = D_{2m\theta}D_{2l\hbar} \otimes U_{4ml\theta}$, with $U_{4ml\theta} := |0\rangle\langle 0| + e^{i4ml\theta}|1\rangle\langle 1|$. In other words, the phase $\Psi = 4ml\theta$ is transferred from the OAM to the control qubit, in the same way as in the geometric phase setup in Refs. [29,32]. By measuring the control qubit, it is then possible to estimate the phase Ψ and to compute θ as $\theta = \Psi/4ml$. Crucially, we engineer an effective generator whose norm scales as $4ml$ by applying two noncommutative operations, i.e., $2m$ rotation operations and $2l$ OAM shift. The observed nonlinear scaling can be interpreted by a reexamination of the Heisenberg uncertainty principle (HUP). That is, when encoding a parameter θ via a rotating gate U_θ, the HUP does not pose an absolute constraint on the vanishing speed of $\delta\theta$ with increasing probe particles or evolution gates; nevertheless, the parameter-based HUP expressed as $\delta\theta \cdot \Delta h \geq \frac{1}{2}$ has to be satisfied [35]. In this trade-off relation, Δh represents the standard deviation (SD) of the infinitesimal translation generator $\hat{h}$ defined as $\hat{h} = i[\partial_\theta U_\theta]U_\theta^\dagger$. In this sense, increasing Δh could minimize the uncertainty in estimating θ.

For a conventional scheme of multipass (MP) encoding, e.g., applying m rotating gates to a l-level OAM beam results in a generator $h_{\rm MP} = i[\partial_\theta(U_\theta^{(m)})](U_\theta^{(m)})^\dagger = \frac{2m\hat{L}_z}{\hbar}$, of which the SD is independent of l and calculated as $\Delta h_{\rm MP} = \frac{2m\Delta L_z}{\hbar}$, with ΔL_z representing the average uncertainty of the initial OAM state (see Appendix A for detailed calculation).

In our quantum switch scheme, the SD of the generator $h_{\rm QS} = i[\partial_\theta W_{\rm QS}]W_{\rm QS}^\dagger$ is calculated as $\Delta h_{\rm QS} = 2m\frac{\Delta L_z}{\hbar} + 2ml$, in which the nonlinear item $2ml$ arises with the factors m and l both representing the gate query times in encoding (see Appendix A for detailed calculation). Accordingly, $\delta\theta$ can vanish with a nonlinear scaling as $\frac{1}{ml}$ while keeping the parameter-based HUP valid. This result is consistent with our previous work in which the gate query times are both N and hence the precision attains the scaling of $\frac{1}{N^2}$ [32].

In our experiment, the hybrid quantum switch is constructed by using the photon polarization as the control qubit to realize the superposition of two alternative orders. The coherent control arises from the spin-orbital coupling [36] introduced by a Q-plate, which couples the OAM and polarization degrees of freedom as

$$Q_l = D_{l\hbar} \otimes |R\rangle\langle L| + D_{l\hbar}^\dagger \otimes |L\rangle\langle R|, \tag{2}$$

where $|L\rangle$ and $|R\rangle$ refer to the left- and right-handed circularly polarized states, respectively. After passing the Q-plate, the $|L\rangle$ and $|R\rangle$ components of a linear polarized photon experience opposite OAM operations as $\pm l\hbar$, with the relative OAM displacement identified to be $2l\hbar$.

The unknown rotation operations are implemented through $m/2$ (m is an even number) pairs of Dove prisms, and each pair consists of one rotatable prism aligned with a relative angle θ to the other stationary prism (see Appendix B for details). The transverse mode of photons rotates 2θ after passing each pair of prisms.

The setup is shown in Fig. 2, and the quantum switch in our experiment is realized through a colinear and round-trip interferometer, which is distinct from previous apparatuses, in which the two orders propagate through two spatially separated arms [18,25,32]. The round-trip

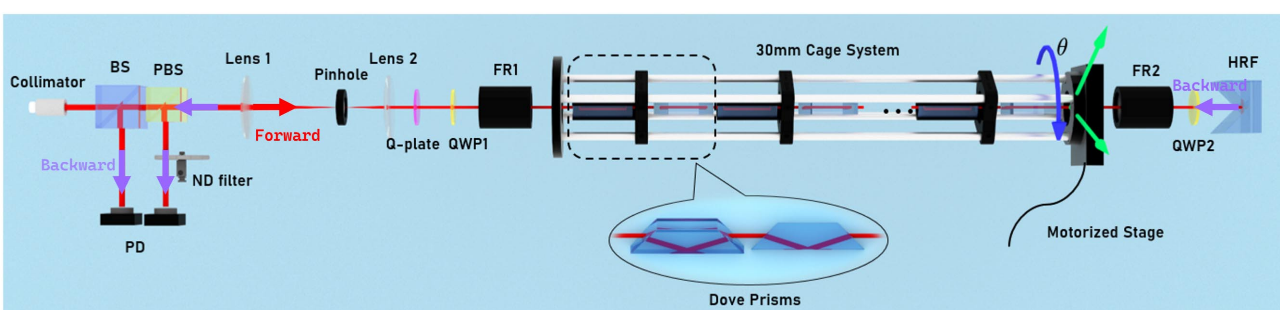

FIG. 2. Experimental setup of the hybrid quantum switch for the measurement of a rotation angle. Our setup uses the photon polarization to control the order of two opposite shifts of the orbital angular momentum. These shifts are performed before and after an unknown transversal rotation, reproducing the same overall dynamics arising from the quantum switch of discrete and continuous variables. The outcome state from the quantum switch acquires a geometric phase of $4ml\theta$ on polarization but no topological charge of OAM. The transverse wave function $|\Phi\rangle$ undergoes 2θ rotation, which can be acquired by detecting the accumulated phase on the control qubit via a projective measurement, while $|\Phi\rangle$ is discarded in the measurement (see Appendix B for details). QWP, quarter wave plate; HRP, hollow roof prism; FR, Faraday rotator; BS, nonpolarizing beamsplitter; PBS, polarization beamsplitter; PD, photon detectors.

configuration effectively mitigates imperfections in the rotation operations induced by the Dove prism, thereby preserving coherence between the two alternative gate orders. After passing the round trip including a l-order Q-plate and m Dove prisms, a horizontally polarized photon experiences $2m\theta$ angular displacement (due to the double pass of Dove prisms) and $2l\hbar$ relative OAM displacement. The control-system joint state evolves as

$$\begin{aligned} & Q_l D_{2m\theta} Q_l |H\rangle|\Phi\rangle \\ &= \frac{1}{\sqrt{2}}(D^{\dagger}_{l\hbar} D_{2m\theta} D_{l\hbar}|\Phi\rangle \otimes |L\rangle + D_{l\hbar} D_{2m\theta} D^{\dagger}_{l\hbar}|\Phi\rangle \otimes |R\rangle) \\ &= \frac{1}{\sqrt{2}}(e^{-2iml\theta}|L\rangle + e^{2iml\theta}|R\rangle) \otimes D_{2m\theta}|\Phi\rangle, \end{aligned} \tag{3}$$

where $|H\rangle$ denotes the horizontally polarized state, and $|\Phi\rangle$ denotes the spatial wave function of photons. In this process, $D_{l\hbar}$ and $D^{\dagger}_{l\hbar}$ are exchanged in different causal orders.

The final estimation of θ is achieved by projecting the control qubit to $|V\rangle\langle V|$, for which the probability should be calculated as

$$P(\theta) = \frac{1}{2}[1 - \cos(4ml\theta + \varphi_0)], \tag{4}$$

where φ_0 represents an initial phase. The value of θ can be directly extrapolated from the projective measurement on the control qubit, while the spatial mode is completely discarded to avoid the complicated measurement of the spatial distribution, which may introduce more technical noise. Most of all, the factor $4ml\theta$ indicates a nonlinear quantum enhancement of the measurement precision of θ while no classical nonlinearity is involved.

To prove the quantum nonlinear enhancement, various values of m and l are tested in our experiment and Fig. 3 shows the interference fringe predicted by Eq. (4). It can be seen that for each pairing of (m, l), the measured projecting probabilities drop on the theoretical curve.

A theoretical analysis shows that the Fisher information of our scheme is calculated as $16\nu m^2 l^2$ (see Appendix C for details), and the theoretical precision to estimate θ can then be obtained from the Cramér-Rao bound and written as

$$\delta\theta \geq \frac{1}{4\sqrt{\nu} ml}, \tag{5}$$

where ν is the photon number used in each trial of measurement.

For each pairing of (m, l), $P(\theta)$ is measured by using approximately 7×10^7 photons to get one estimation of θ from Eq. (4). The true value and uncertainty of θ are identified as the mean and root mean square error (RMSE) of 60 trials of estimation. The RMSE with various $4ml$ is given in Fig. 4, which approaches the Cramér-Rao bound and vanishes with the speed $1/4ml$, as predicted by Eq. (5). The experimental fitting curve is only worse than the Cramér-Rao bound by approximately a factor of 2.5, which is mainly due to the noise when mechanical rolling Dove prisms. The ultimate precision is obtained by using a 128-order Q-plate and four pairs of Dove prisms, which jointly promise an enhanced factor as high as 4096 and practically achieve 2317 in the experiment. When

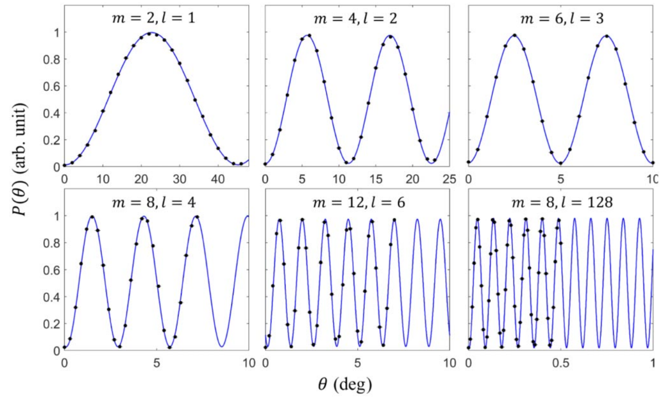

FIG. 3. The interference fringe derived from the geometric phase on the control qubit. The projection probability $P(\theta)$ is measured by changing θ, for which the data points are fitted with the function given by Eq. (4), and the fitting curves are shown in blue. A total of six combinations of m, l are investigated, and the period reducing with the scaling of $1/ml$ indicates the nonlinearly enhanced precision to measure θ. In each trial of the experiment, $P(\theta)$ is calculated from the results of projective measurement on $\nu = 7 \times 10^7$ photons, and the data points denote the mean values ($\pm$RMSE) of 60 trials of the experiment. As we can see, all the data points fall at the fitting curve and the error bar is not visible since the error is smaller than the dot size.

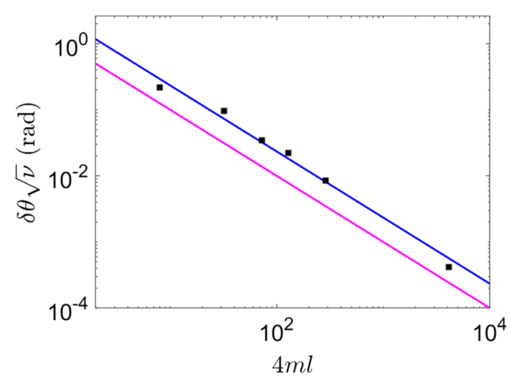

FIG. 4. Nonlinear scaling of the measurement precision normalized for one photon. The black data points are the measured RMSE $\delta\theta$ normalized by the square root of photon number ν, which represents the measurement precision achieved with one photon for varying $4ml$. The blue fitting line is close to the theoretical Cramér-Rao bound $\delta\theta\sqrt{\nu} = \frac{1}{4ml}$ (red line), with a gap factor of 2.4.

measuring a rotating angle of $0.025°$ with 7.16×10^7 photons, the absolute precision is up to $0.0105''$ corresponding to a normalized precision of 4.3×10^{-4} rad for one photon. Both the enhancement factor and the normalized precision achieved in this study significantly surpass those obtained in the indefinite evolution scheme that employs a reversing operation on OAM beams [37], as well as those in the classical scheme named photonic gear [38], which aims to measure the relative rotation between two reference frames responsible for state preparation and measurement, respectively. By contrast, our proposed scheme addresses more general scenarios where a rotating object is completely isolated from the entire apparatus. In practice, scaling up the enhanced factor faces inherent physical limitations. For example, increasing the parameter l excites higher-order spatial modes, which generally suffer from reduced fidelity and are more challenging to preserve and transmit [39–41]. Moreover, increasing m introduces additional photon loss owing to the insertion loss of the prism; beyond a certain threshold, this loss outweighs the intended enhancement, thereby negating the net benefit conferred by the added prism.

III. DISCUSSION

Classical nonlinear interactions among N particles are known to lead to a nonlinear scaling of the measurement uncertainty as $\Delta \propto 1/N^{\frac{3}{2}}$ [42–45]. However, such enhancements typically do not apply to the basic scenario of N independent and identical processes, and have been subject to dispute [46–48]; especially, nonlinear interactions have been found to be unable to break the classical limit in terms of relevant resources such as the energy of the probes [47,48] and universal resource count [7,46]. Although our scheme does not rely on a specific probing mechanism and thus lacks a fixed initial energy budget for defining the scaling behavior, it nonetheless follows a $1/ml$ nonlinear scaling law with respect to the total count of universal resources (see Appendix A). In stark contrast to the nonlinear interaction scheme, our scheme only harnesses noninteracting photons and independent processes.

Notably, noncommutativity constitutes the fundamental quantum resource enabling the precision enhancement in the present protocol, while the ICO structure serves as a novel operational framework that fully harnesses this resource and renders the protocol experimentally feasible, especially without requiring exotic state preparation or information-losing measurements. Our approach is fundamentally different from conventional metrology schemes, such as the strategy of increasing ΔL_z to yield a large SD of the generator exemplified by Δh_{MP}, and then boosting the quantum Fisher information. For such a scheme, the optimal measurement is formidably hard since it requires projective measurement to a superposition state of two OAM eigenmodes without photon loss [39,49]. Applying multipass rotating gates in interferometers with separated arms [37,50] renders QFI only a quarter of that in our scheme (see Appendix C for detailed analysis). Furthermore, these schemes fail to provide a practically competitive level of precision, since a high interferometric visibility in these schemes is tightly contingent on preparing an initial OAM mode with perfect rotational symmetry [51–55]. Our approach releases the requirement to prepare a specific quantum state with high quality. Physically, the order of the Q-plates and the number of Dove prisms play a crucial role, whereas the input state can be arbitrary—even a scrambled speckle pattern yields identical results. For the information extraction, ICO encodes the parameter to the relative phase of the control qubit, and the optimal projective measurement can be simply executed with a polarizer. Moreover, other faults for the interferometer with separated arms, e.g., the path deviation, the phase offset, and the polarization deflection, can also be overcome in our colinear and round-trip configuration.

Considering that quantum resources are counted as the number of used gates in the evolution, the power of our scheme can be characterized as the normalized precision achieved by one photon, which attains quantum nonlinear scaling of $1/4ml$ and achieves 4.3×10^{-4} rad in the rotation angle measurement. The overall RMSE reduces with the increasing photon number ν, while merely showing a classical scaling of $1/\sqrt{\nu}$. Our scheme, experimentally demonstrated for rotations on an OAM system, can in principle be applied to the problem of phase estimation, or the estimation of other shift parameters associated with a generator with a discrete spectrum. Overall, the framework and experimental techniques developed here open up new opportunities to advance the frontier of precision measurements in quantum technologies.

ACKNOWLEDGMENTS

This work was supported by the National Natural Science Foundation of China (Grants No. 12350006 and No. 92576202), Quantum Science and Technology-National Science and Technology Major Project (No. 2021ZD0301200), the National Natural Science Foundation of China via Excellent Young Scientists Fund (Hong Kong and Macau) Project 12322516, the Hong Kong Research Grant Council (RGC) through the Early Career Scheme (ECS) Grant No. 27310822 and the General Research Fund (GRF) Grant No. 17303923, the Fundamental Research Funds for the Central Universities (Grant No. YD2030002026), by the Hong Kong Research Grant Council through Grants No. T45-406/23-R and No. R7035-21F, by the Ministry of Science and Technology of China through Grant No. 2023ZD0300600, and by the John Templeton Foundation through Grant No. 62312, The Quantum Information Structure of Spacetime (qiss.fr). The opinions expressed in this publication are those of the authors and do not necessarily reflect the views of the John Templeton Foundation. Research at the Perimeter Institute is supported by the Government of Canada through the Department of Innovation, Science and Economic Development Canada and by the Province of Ontario through the Ministry of Research, Innovation and Science.

DATA AVAILABILITY

The data that support the findings of this article are not publicly available because they contain commercially sensitive information. The data are available from the authors upon reasonable request.

APPENDIX A: CALCULATION OF GENERATORS FOR CONVENTIONAL AND ICO SCHEMES

In quantum metrology, measurement protocols generally follow a definite causal order. Take a conventional process as an example, where OAM shifting is performed first, followed by rotation. This process is represented as $U_\theta^{(m)} = (D_{2\theta})^m D_{2l\hbar}$. The generator of the entire process can be derived as follows:

$$h_{\mathrm{MP}} = i[\partial_\theta U_c]U_c^\dagger = i[\partial_\theta D_{2m\theta}]D_{2m\theta}^\dagger = \frac{2m\hat{L}_z}{\hbar}. \tag{A1}$$

Subsequently, the precision of parameter estimation can be obtained through this generator and is expressed as $\delta\theta_c \geq \frac{1}{4m\Delta L_z}$. In this bound, the precision is determined by the variance of $\hat{L}_z$ in the probe state.

In the quantum switch protocol, the system's evolution is governed by the unitary operator $W_{\mathrm{QS}} = (D_{2\hbar})^l(D_{2\theta})^m \otimes |0\rangle\langle 0| + (D_{2\theta})^m(D_{2\hbar})^l \otimes |1\rangle\langle 1|$, where m and l are the numbers of queries for the respective evolution processes. The corresponding generator within the ICO process can be formally expressed as

$$\begin{aligned} h_{\mathrm{QS}} &= i[\partial_\theta W_{\mathrm{QS}}]W_{\mathrm{QS}}^\dagger \\ &= \frac{2m}{\hbar}[\hat{L}_z \otimes |0\rangle\langle 0| + D_{2l\hbar}\hat{L}_z D_{2l\hbar}^\dagger \otimes |1\rangle\langle 1|] \\ &= 2m\left(\frac{\hat{L}_z}{\hbar} + l\right) - 2ml\hat{\sigma}_z. \end{aligned} \tag{A2}$$

Under this framework, the control qubits are initialized in the superposition state $\frac{1}{2}(|0\rangle + |1\rangle)$, which remains fixed throughout the protocol. The resultant precision scaling is quantified by the quantum Cramér-Rao bound $\delta\theta \geq \frac{1}{4m\Delta L_z/\hbar + 4ml}$. The generator of the quantum switch protocol, characterized by $\Delta h_{\mathrm{QS}} = 2m\frac{\Delta\hat{L}_z}{\hbar} + 2ml$, introduces a fundamental distinction from conventional quantum metrology paradigms. Notably, the emergence of the additional term $2ml$, arising from coherent control of gate order, demonstrates that the intrinsic uncertainty inherent in the process constitutes a non-negligible contribution to the final precision limit. The nonlinear term $2ml$ is also consistent with the bound $\delta\theta \geq \frac{1}{2|\langle H\rangle|}$ defined in the context of universal count, where $|\langle H\rangle|$ denotes the expectation value of the generator. This expectation value can be derived as $|\langle H\rangle| = \langle H\rangle - \lambda_{\min} = 2m\frac{|\langle\hat{L}_z\rangle|}{\hbar} + 2ml$, with $\lambda_{\min}$ being the minimum eigenvalue of the generator. Since the initial probe in our experiment is prepared as a Gaussian mode with $\langle\hat{L}_z\rangle = 0$, both the term $|\langle\hat{L}_z\rangle|$ and $\Delta\hat{L}_z$ vanish. Consequently, the universal resource count yields the same nonlinear bound $1/(4ml)$, which coincides with the quantum Cramér-Rao bound.

APPENDIX B: DETAILS OF EXPERIMENT SETUP

1. System overview

As shown in Fig. 5, a collinear round-trip configuration of the quantum switch is implemented to simultaneously cancel experimental imperfections in rotation operations and double their effective application. To clarify the experimental protocol, the complete procedure is systematically outlined below:

First, half of the photons from a DFB laser transmit the beam splitter (BS) and become horizontally polarized after passing the polarization beam splitter (PBS), which can be written into the superposition of left- and right-handed circular polarization as $\frac{1}{\sqrt{2}}(|R\rangle + |L\rangle)$ and serves as the control qubit. A Q-plate couples the spin-orbital momentum to create a joint quantum state as $\frac{1}{\sqrt{2}}(|R\rangle| + l\rangle + |L\rangle| - l\rangle)$ and thus introduces $2l\hbar$ relative OAM displacement between the two orders.

After that, a 0° QWP and a $\pi/4$ FR, namely, the QWP1-FR1 suite, transform circular polarization to linear polarization ($|R\rangle \to |V\rangle$ and $|L\rangle \to |H\rangle$), and then $m/2$ pairs of Dove prisms rotate the transversal mode for both orders to encode θ to the joint state $\frac{1}{\sqrt{2}}(e^{-iml\theta}|V\rangle| + l\rangle + e^{iml\theta}|H\rangle| - l\rangle)$. Each pair of Dove prisms includes a stationary prism and the other rotatable prism, as shown in the inset. A $\pi/4$ FR and a following 0° QWP (FR2-QWP2) conduct the linear-to-circular transformation of the photon polarization, and the ending hollow roof prism (HRP) flips the circular polarization without inversion of OAM. The reflected photons exchange the linear polarization ($|V\rangle \to -|H\rangle$ and $|H\rangle \to |V\rangle$) after repassing the FR2-QWP2 suite; and thus, the polarization deflection due to the internal reflection on the prisms is eliminated, and the control qubit is protected to proceed with the quantum switch. After reversely passing the Dove prisms, the photons undergo twofold rotating operations and joint state changes to $\frac{1}{\sqrt{2}}(-e^{-2iml\theta}|H\rangle| + l\rangle + e^{2iml\theta}|V\rangle| - l\rangle)$. Then the FR1-QWP1 suite retrieves the linear polarization

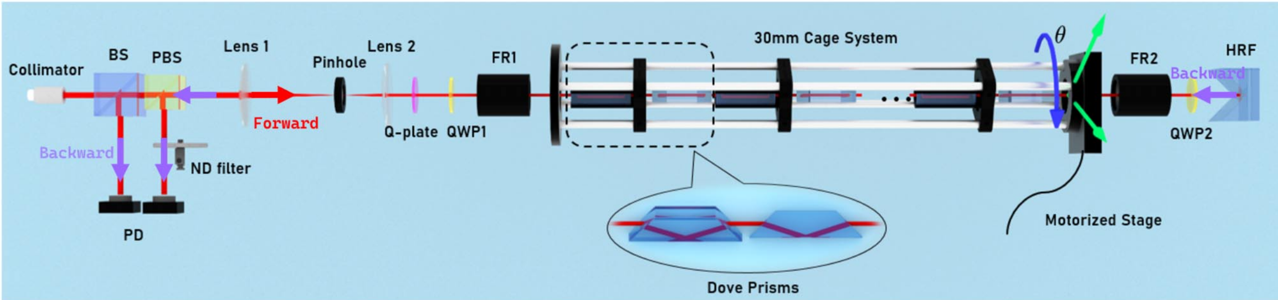

FIG. 5. The same as the experiment setup figure in the main text.

to circular polarization, and the joint state evolves to $\frac{1}{\sqrt{2}}(-e^{-2iml\theta}|R\rangle|+l\rangle + e^{2iml\theta}|L\rangle|-l\rangle)$. Once again, the Q-plate introduces the spin-orbital coupling but oppositely for the two orders, and the outcome state from the quantum switch is $\frac{1}{\sqrt{2}}(e^{-2iml\theta}|L\rangle + e^{2iml\theta}|R\rangle)$, which acquires a geometric phase of $4ml\theta$ but no topological charge of OAM. The transverse wave function $|\Phi\rangle$ undergoes 2θ rotation and is not measured. After being spatially filtered by the pinhole placed on the common focal plane of Lens 1 and Lens 2, photons exiting from the reflection ports of the PBS and BS are recorded by two photodiodes (PDs) to calculate the projecting probability $P(\theta)$, and the ND filter is used to balance the collection efficiency between the two ports.

2. Details of the rotating system

To transmit OAM beam below 128th order, Dove prisms with 5×5 mm clear aperture are used. All the rotatable Dove prisms are aligned with an established line by a 30 mm cage system, which can be rotated through a motorized rotation stage. The initial angle of Dove prisms does not influence the result since it can always be made zero through QWP1. The visibility of interference between two circularly polarized states is approximately 0.96 after being improved by a spatial filter system consisting of two lenses and a pinhole. The focus lengths of Lens 1 and Lens 2 are $f = 10$ cm and $f = 5$ cm, respectively, which are used to focus and collimate the beam. The pinhole is placed in the common focus of the lenses to block the stray light due to the unflatness of the reflecting surface. For a 128-order OAM beam suffering a large radius and divergence angle, we exchange the position of Lens 1 and Lens 2 to expand the incident beam and change the pinhole size to $200\,\mu$m. The Dove prism size is changed to 10×10 mm to accommodate the large profile of OAM beam.

3. Necessity of the hollow roof prism

Unlike the usual usage of the HRP to introduce an optical delay, the beam shining on the HRP is centered around the dihedral line (roof joint) so the reflected beam exactly overlaps with the incident beam. The dihedral line inevitably causes single-slit diffraction, which can be spatially filtered by the pinhole.

The HRP meanwhile reverses wave vector k and reflects the y coordinate, and its operator Π can be defined via $\Pi|x\rangle \otimes |y\rangle \otimes |k\rangle = |x\rangle \otimes |-y\rangle \otimes |-k\rangle$. One horizontally placed Dove prism merely reflects the y coordinate of a photon and can be expressed as $P|x\rangle \otimes |y\rangle \otimes |k\rangle = |x\rangle \otimes |-y\rangle \otimes |k\rangle$; and rotating the Dove prism by an angle of θ, the operation becomes $P_\theta = R^\dagger(\theta)PR(\theta)$. The action of a pair of Dove prisms on the forward and backward paths can be written as $PP_\theta = R(2\theta)$ and $P_\theta P = R^\dagger(2\theta)$, respectively. Thus, a round trip consisting of $m/2$ (m is an even number) pairs of Dove prisms and one HRP eventually rotates the photon by $2m\theta$, since we have

$$R^\dagger(m\theta)\Pi R(m\theta) = \Pi R(2m\theta). \tag{B1}$$

In contrast, a normal mirror acts as $R^\dagger(2\theta)R(2\theta) = I$ and fails to encode the parameter to be measured.

4. The Jones matrix of Dove prism

The photon propagating through a Dove prism experiences twice refraction on the incident and exit planes (labeled as plane 1 and plane 3 in Fig. 6), and one time of total inner reflection on the bottom plane (labeled as plane2 in Fig. 6). Both photon loss and polarization alteration occur during the transmission of a Dove prism, which cannot be represented by a unitary transformation.

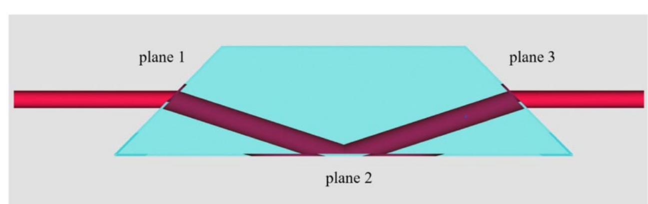

FIG. 6. Photon transmission through horizontally placed Dove prism. The incident photon is refracted at plane 1 and then totally reflected at the inner plane 2, and finally exits the prism after being refracted at plane 3.

An alternative way to describe this process is using the Jones matrix, which can be derived from Fresnel formulas. When the Dove prism is horizontally placed, the Jones matrix can be written as

$$J(0) = \begin{bmatrix} t_3^s r_2^s t_1^s & 0 \\ 0 & t_3^p r_2^p t_1^p \end{bmatrix}, \tag{B2}$$

in which $t_i^{s/p}(r_i^{s/p})$ represents the transmission (reflection) coefficient of s/p wave on the ith plane. When Dove prism is rotated by an angle θ, the Jones matrix changes to [56]:

$$\begin{aligned} J(\theta) &= R^\dagger(\theta)J(0)R(\theta) \\ &= \begin{bmatrix} \tau_s\cos^2\theta + \tau_p\sin^2\theta & (\tau_s-\tau_p)\cos\theta\sin\theta \\ (\tau_p-\tau_s)\cos\theta\sin\theta & \tau_s\sin^2\theta+\tau_p\cos^2\theta \end{bmatrix}, \end{aligned} \tag{B3}$$

where τ_s and τ_p stand for $t_{3s}r_{2s}t_{1s}$ and $t_{3p}r_{2p}t_{1p}$, respectively, and $R(\theta)$ is the SO(2) rotation matrix. Then, we find the conclusion that $J(\theta)\cdot J(\theta+\frac{\pi}{2}) \propto I$ from the expression of $J(\theta)$ in Eq. (B3).

5. Protecting the control qubit against polarization deflection on prisms

Dove prism introduces an extra phase and amplitude difference between the s-wave and the p-wave when the total internal reflection occurs on the bottom surface. This polarization-dependent transmission necessarily changes the polarization state of photons which serves as the control qubit of the quantum switch, and diminishes the interference visibility between the two orders. This polarization deflection cannot be precompensated or postcompensated since the Jones matrix of Dove prism $J(\alpha)$ also hinges on the unknown θ (see Appendix B 5). We develop a method to eliminate this deflection by exploiting the relation that $J(\alpha)J(\alpha+\pi/2)$ is proportional to a unit matrix I, where α is the angle between the axis of Dove prism and polarization of photons. This relation suggests that any depolarization can be eliminated after double passing the prism with orthogonal polarization.

The polarization flipping suite can be realized through a 0° aligned QWP and a following FR rotating the photon polarization by 45°. Double pass of one such suite before the ending HRP flips the photon polarization; and thus, the Jones matrix of m pairs of Dove prism can be written as $J_m(\theta)\ldots J_2(\theta)J_1(\theta)$ and $J_1(\theta+\pi/2)J_2(\theta+\pi/2)\ldots J_m(\theta+\pi/2)$ for the forward and backward trips, respectively, which jointly result in an identity.

APPENDIX C: FISHER INFORMATION CALCULATION

The geometric phase imposed on the control qubit in the state $(|0\rangle+|1\rangle)$ serves as a pointer for measuring θ, and the extractable Fisher information by measuring this phase is proportional to ml. When we input a state $(|0\rangle+|1\rangle)\otimes|\Phi_i\rangle$, the output state after all the quantum switch is written as

$$\begin{aligned} |\Psi_f\rangle &= (D_{l\hbar}^\dagger D_{2m\theta}D_{l\hbar}|0\rangle + D_{l\hbar}D_{2m\theta}D_{l\hbar}^\dagger|1\rangle)\otimes|\Phi_i\rangle \\ &= (e^{-i2ml\theta}|0\rangle + e^{i2ml\theta}|1\rangle)\otimes D_{m\theta}|\Phi_i\rangle \\ &= |\varphi_f\rangle\otimes|\Phi_f\rangle, \end{aligned}$$

where $|\psi_f\rangle$ is the output state of the pointer, and $|\Phi_i\rangle$ and $|\Phi_f\rangle$ are the initial and final states of the system. Then, a direct calculation of quantum Fisher information (QFI) is given by [57,58]:

$$Q_\theta = 4(\langle\partial_\theta\Psi_f|\partial_\theta\Psi_f\rangle - \langle\partial_\theta\Psi_f|\Psi_f\rangle\langle\Psi_f|\partial_\theta\Psi_f\rangle). \tag{C2}$$

Here, we have the derivation $|\partial_\theta\Psi_f\rangle = |\partial_\theta\varphi_f\rangle\otimes|\Phi_f\rangle + |\varphi_f\rangle\otimes|\partial_\theta\Phi_f\rangle$. Thus, the quantum Fisher information can be divided into two parts:

$$Q_\theta = Q_\theta^p + Q_\theta^s. \tag{C3}$$

The first term is calculated as $Q_\theta^p = 16\ m^2l^2$ and can be extracted by measuring the pointer state. The second term Q_θ^s represents the QFI of the system state, which is related to the final distribution of photon transverse mode. In the sense that the transverse mode is discarded in the final measurement, the specific form of Q_θ^s is not of interest here.

To saturate the QFI, we project the pointer to $|\pm\rangle$ and the theoretical probabilities are calculated as $P_\pm(\theta) = \frac{1}{2}[1\pm\cos(4ml\theta)]$. The extracted Fisher information is then given by

$$F_\theta^p = \frac{1}{P_+(\theta)}\left[\frac{\partial P_+(\theta)}{\partial\theta}\right]^2 + \frac{1}{P_-(\theta)}\left[\frac{\partial P_-(\theta)}{\partial\theta}\right]^2 = 16\ m^2l^2. \tag{C4}$$

From the Cramér-Rao bound, the RMSE to estimate θ satisfies

$$\delta\theta \geq \frac{1}{\sqrt{\nu F_\theta}} = \frac{1}{4\sqrt{\nu}ml}, \tag{C5}$$

which indicates that the nonlinear enhanced precision can be attained by the projective measurement on the control qubit.

The nonlinear precision enhancement cannot be achieved solely through the OAM shifting operation without coherent control of gate order. When considering that an l-order OAM state is generated by an OAM shifting followed by an unknown rotation, the state after applying fixed-order gates can be expressed as

$$\begin{aligned} Q_\theta(|\psi_{\text{fixed}}\rangle) &= 4\langle +l|(\partial_\theta D_{2m\theta})(\partial_\theta D^\dagger_{2m\theta})|+l\rangle \\ &\quad - 4|\langle +l|\partial_\theta D^\dagger_{2m\theta}|+l\rangle|^2 \\ &= 4\cdot(4\ m^2 l^2) - 4\cdot(2ml)^2 \\ &= 0. \end{aligned} \tag{C6}$$

The result of zero quantum Fisher information indicates that no information regarding θ can be extracted in this fixed process. This outcome is readily understandable, as the rotational transformation applied to the OAM eigenstate introduces an additional global phase factor that is not directly observable. It is also significant to note that in our experiment, l refers to the order of the OAM shift gate rather than the order of OAM eigenstates; thus, any arbitrary input system state will consistently map to the same measurement result.

Considering an alternative experimental configuration of the Mach-Zehnder (MZ) interferometer [50], a photon is prepared in a superposition of two paths. In this setup, one path undergoes a rotation operation while the other remains unchanged. The process can be described by the expression $D_{2m\theta}|0\rangle\langle 0| + |1\rangle\langle 1|$. Starting with an initial state $|+l\rangle$ and employing the path state $\frac{1}{\sqrt{2}}(|0\rangle + |1\rangle)$, the joint state of the system and path after applying the rotation operation can be expressed as

$$|\Phi_f\rangle = \frac{1}{\sqrt{2}}(D_{2m\theta}|+l\rangle|0\rangle + |+l\rangle|1\rangle). \tag{C7}$$

Then, the QFI is calculated via Eq. (C2) as

$$Q_\theta(\Phi_f) = 4\left(2m^2l^2\theta^2 - \left|\frac{1}{2}i2ml\theta\right|^2\right) = 4m^2l^2\theta^2, \tag{C8}$$

where it is noted that the QFI for this MZ interference configuration is only one quarter of that obtained from a quantum switch configuration. Furthermore, it should be emphasized that the visibility of MZ interferometry is limited by the rotational symmetry inherent in the input beam distribution; thus, theoretically calculated QFI cannot be fully realized under conditions of imperfect state preparation.

[1] V. Giovannetti, S. Lloyd, and L. Maccone, Quantum-enhanced measurements: Beating the standard quantum limit, Science **306**, 1330 (2004).

[2] V. Giovannetti, S. Lloyd, and L. Maccone, Quantum metrology, Phys. Rev. Lett. **96**, 010401 (2006).

[3] J. J. Bollinger, W. M. Itano, D. J. Wineland, and D. J. Heinzen, Optimal frequency measurements with maximally correlated states, Phys. Rev. A **54**, R4649 (1996).

[4] I. Afek, O. Ambar, and Y. Silberberg, High-noon states by mixing quantum and classical light, Science **328**, 879 (2010).

[5] T. Nagata, R. Okamoto, J. L. O'Brien, K. Sasaki, and S. Takeuchi, Beating the standard quantum limit with four-entangled photons, Science **316**, 726 (2007).

[6] P. Grangier, R. E. Slusher, B. Yurke, and A. LaPorta, Squeezed-light–enhanced polarization interferometer, Phys. Rev. Lett. **59**, 2153 (1987).

[7] M. Zwierz, C. A. Pérez-Delgado, and P. Kok, General optimality of the Heisenberg limit for quantum metrology, Phys. Rev. Lett. **105**, 180402 (2010).

[8] P. Thomas, L. Ruscio, O. Morin, and G. Rempe, Efficient generation of entangled multiphoton graph states from a single atom, Nature (London) **608**, 677 (2022).

[9] X.-L. Wang, Y.-H. Luo, H.-L. Huang, M.-C. Chen, Z.-E. Su, C. Liu, C. Chen, W. Li, Y.-Q. Fang, X. Jiang *et al.*, 18-qubit entanglement with six photons' three degrees of freedom, Phys. Rev. Lett. **120**, 260502 (2018).

[10] R. Demkowicz-Dobrzański, K. Banaszek, and R. Schnabel, Fundamental quantum interferometry bound for the squeezed-light-enhanced gravitational wave detector geo 600, Phys. Rev. A **88**, 041802(R) (2013).

[11] G. Chen, L. Zhang, W.-H. Zhang, X.-X. Peng, L. Xu, Z.-D. Liu, X.-Y. Xu, J.-S. Tang, Y.-N. Sun, D.-Y. He *et al.*, Achieving Heisenberg-scaling precision with projective measurement on single photons, Phys. Rev. Lett. **121**, 060506 (2018).

[12] G. Chen, N. Aharon, Y.-N. Sun, Z.-H. Zhang, W.-H. Zhang, D.-Y. He, J.-S. Tang, X.-Y. Xu, Y. Kedem, C.-F. Li *et al.*, Heisenberg-scaling measurement of the single-photon Kerr non-linearity using mixed states, Nat. Commun. **9**, 1 (2018).

[13] L. Hardy, Towards quantum gravity: A framework for probabilistic theories with non-fixed causal structure, J. Phys. A **40**, 3081 (2007).

[14] O. Oreshkov, F. Costa, and Č. Brukner, Quantum correlations with no causal order, Nat. Commun. **3**, 1092 (2012).

[15] G. Chiribella, G. M. D'Ariano, P. Perinotti, and B. Valiron, Quantum computations without definite causal structure, Phys. Rev. A **88**, 022318 (2013).

[16] L. A. Rozema, T. Strömberg, H. Cao, Y. Guo, B.-H. Liu, and P. Walther, Experimental aspects of indefinite causal order in quantum mechanics, Nat. Rev. Phys. **6**, 483 (2024).

[17] G. Chiribella, Perfect discrimination of no-signalling channels via quantum superposition of causal structures, Phys. Rev. A **86**, 040301(R) (2012).

[18] L. M. Procopio, A. Moqanaki, M. Araújo, F. Costa, I. A. Calafell, E. G. Dowd, D. R. Hamel, L. A. Rozema, Č. Brukner, and P. Walther, Experimental superposition of orders of quantum gates, Nat. Commun. **6**, 1 (2015).

[19] T. Colnaghi, G. M. D'Ariano, S. Facchini, and P. Perinotti, Quantum computation with programmable connections between gates, Phys. Lett. A **376**, 2940 (2012).

[20] M. Araújo, F. Costa, and Č. Brukner, Computational advantage from quantum-controlled ordering of gates, Phys. Rev. Lett. **113**, 250402 (2014).

[21] M. J. Renner and Č. Brukner, Computational advantage from a quantum superposition of qubit gate orders, Phys. Rev. Lett. **128**, 230503 (2022).

[22] D. Ebler, S. Salek, and G. Chiribella, Enhanced communication with the assistance of indefinite causal order, Phys. Rev. Lett. **120**, 120502 (2018).

[23] K. Goswami, Y. Cao, G. A. Paz-Silva, J. Romero, and A. G. White, Increasing communication capacity via superposition of order, Phys. Rev. Res. **2**, 033292 (2020).

[24] G. Chiribella, M. Wilson, and H. F. Chau, Quantum and classical data transmission through completely depolarizing channels in a superposition of cyclic orders, Phys. Rev. Lett. **127**, 190502 (2021).

[25] Y. Guo, X.-M. Hu, Z.-B. Hou, H. Cao, J.-M. Cui, B.-H. Liu, Y.-F. Huang, C.-F. Li, G.-C. Guo, and G. Chiribella, Experimental transmission of quantum information using a superposition of causal orders, Phys. Rev. Lett. **124**, 030502 (2020).

[26] D. Felce and V. Vedral, Quantum refrigeration with indefinite causal order, Phys. Rev. Lett. **125**, 070603 (2020).

[27] G. Zhu, Y. Chen, Y. Hasegawa, and P. Xue, Charging quantum batteries via indefinite causal order: Theory and experiment, Phys. Rev. Lett. **131**, 240401 (2023).

[28] Y. Wei, G.-C. Li, L.-W. Wang, X.-S. Hong, L. Chen, S.-Q. Zhang, H.-Q. Xu, Y. Liu, Y.-S. Zhang, G. Chen *et al.*, Direct estimation of quantum channel incompatibility via a quantum switch, Sci. China Inf. Sci. **68**, 180502 (2025).

[29] X. Zhao, Y. Yang, and G. Chiribella, Quantum metrology with indefinite causal order, Phys. Rev. Lett. **124**, 190503 (2020).

[30] F. Chapeau-Blondeau, Noisy quantum metrology with the assistance of indefinite causal order, Phys. Rev. A **103**, 032615 (2021).

[31] M. An, S. Ru, Y. Wang, Y. Yang, F. Wang, P. Zhang, and F. Li, Noisy quantum parameter estimation with indefinite causal order, Phys. Rev. A **109**, 012603 (2024).

[32] P. Yin, X. Zhao, Y. Yang, Y. Guo, W.-H. Zhang, G.-C. Li, Y.-J. Han, B.-H. Liu, J.-S. Xu, G. Chiribella *et al.*, Experimental super-Heisenberg quantum metrology with indefinite gate order, Nat. Phys. **19**, 1122 (2023).

[33] D. Judge, On the uncertainty relation for angle variables, Nuovo Cimento (1955–1965) **31**, 332 (1964).

[34] D. T. Pegg, S. M. Barnett, R. Zambrini, S. Franke-Arnold, and M. Padgett, Minimum uncertainty states of angular momentum and angular position, New J. Phys. **7**, 62 (2005).

[35] Z. Hou, Y. Jin, H. Chen, J.-F. Tang, C.-J. Huang, H. Yuan, G.-Y. Xiang, C.-F. Li, and G.-C. Guo, "Super-Heisenberg" and Heisenberg scalings achieved simultaneously in the estimation of a rotating field, Phys. Rev. Lett. **126**, 070503 (2021).

[36] L. Marrucci, C. Manzo, and D. Paparo, Optical spin-to-orbital angular momentum conversion in inhomogeneous anisotropic media, Phys. Rev. Lett. **96**, 163905 (2006).

[37] B. Xia, J. Huang, H. Li, Z. Luo, and G. Zeng, Nanoradian-scale precision in light rotation measurement via indefinite quantum dynamics, Sci. Adv. **10**, eadm8524 (2024).

[38] V. D'ambrosio, N. Spagnolo, L. Del Re, S. Slussarenko, Y. Li, L. C. Kwek, L. Marrucci, S. P. Walborn, L. Aolita, and F. Sciarrino, Photonic polarization gears for ultra-sensitive angular measurements, Nat. Commun. **4**, 2432 (2013).

[39] E. Bolduc, N. Bent, E. Santamato, E. Karimi, and R. W. Boyd, Exact solution to simultaneous intensity and phase encryption with a single phase-only hologram, Opt. Lett. **38**, 3546 (2013).

[40] N. Bozinovic, Y. Yue, Y. Ren, M. Tur, P. Kristensen, H. Huang, A. E. Willner, and S. Ramachandran, Terabit-scale orbital angular momentum mode division multiplexing in fibers, Science **340**, 1545 (2013).

[41] Y. Ren, H. Huang, G. Xie, N. Ahmed, Y. Yan, B. I. Erkmen, N. Chandrasekaran, M. P. Lavery, N. K. Steinhoff, M. Tur *et al.*, Atmospheric turbulence effects on the performance of a free space optical link employing orbital angular momentum multiplexing, Opt. Lett. **38**, 4062 (2013).

[42] S. Boixo, S. T. Flammia, C. M. Caves, and J. M. Geremia, Generalized limits for single-parameter quantum estimation, Phys. Rev. Lett. **98**, 090401 (2007).

[43] S. M. Roy and S. L. Braunstein, Exponentially enhanced quantum metrology, Phys. Rev. Lett. **100**, 220501 (2008).

[44] S. Choi and B. Sundaram, Bose-Einstein condensate as a nonlinear Ramsey interferometer operating beyond the Heisenberg limit, Phys. Rev. A **77**, 053613 (2008).

[45] M. Napolitano, M. Koschorreck, B. Dubost, N. Behbood, R. J. Sewell, and M. W. Mitchell, Interaction-based quantum metrology showing scaling beyond the Heisenberg limit, Nature (London) **471**, 486 (2011).

[46] M. Zwierz, C. A. Pérez-Delgado, and P. Kok, Ultimate limits to quantum metrology and the meaning of the Heisenberg limit, Phys. Rev. A **85**, 042112 (2012).

[47] D. W. Berry, M. J. W. Hall, M. Zwierz, and H. M. Wiseman, Optimal Heisenberg-style bounds for the average performance of arbitrary phase estimates, Phys. Rev. A **86**, 053813 (2012).

[48] M. J. Hall and H. M. Wiseman, Does nonlinear metrology offer improved resolution? answers from quantum information theory, Phys. Rev. X **2**, 041006 (2012).

[49] N. Bent, H. Qassim, A. Tahir, D. Sych, G. Leuchs, L. L. Sánchez-Soto, E. Karimi, and R. Boyd, Experimental realization of quantum tomography of photonic qudits via symmetric informationally complete positive operator-valued measures, Phys. Rev. X **5**, 041006 (2015).

[50] J. Courtial, K. Dholakia, D. A. Robertson, L. Allen, and M. J. Padgett, Measurement of the rotational frequency shift imparted to a rotating light beam possessing orbital angular momentum, Phys. Rev. Lett. **80**, 3217 (1998).

[51] R. Neo, S. J. Tan, X. Zambrana-Puyalto, S. Leon-Saval, J. Bland-Hawthorn, and G. Molina-Terriza, Correcting vortex splitting in higher order vortex beams, Opt. Express **22**, 9920 (2014).

[52] A. Y. Bekshaev, M. S. Soskin, and M. V. Vasnetsov, Optical vortex symmetry breakdown and decomposition of the orbital angular momentum of light beams, J. Opt. Soc. Am. A **20**, 1635 (2003).

[53] R. Fickler, G. Campbell, B. Buchler, P. K. Lam, and A. Zeilinger, Quantum entanglement of angular momentum states with quantum numbers up to 10,010, Proc. Natl. Acad. Sci. U.S.A. **113**, 13642 (2016).

[54] R. Li, Y. Ren, T. Liu, C. Wang, Z. Liu, J. Zhao, R. Sun, and Z. Wang, Generating large topological charge Laguerre–Gaussian beam based on 4k phase-only spatial light modulator, Chin. Optic. Lett. **20**, 120501 (2022).

[55] J. Pinnell, V. Rodríguez-Fajardo, and A. Forbes, Probing the limits of orbital angular momentum generation and detection with spatial light modulators, J. Opt. **23**, 015602 (2021).

[56] I. Moreno, Jones matrix for image-rotation prisms, Appl. Opt. **43**, 3373 (2004).

[57] C. W. Helstrom, Quantum detection and estimation theory, J. Stat. Phys. **1**, 231 (1969).

[58] A. S. Holevo, *Probabilistic and Statistical Aspects of Quantum Theory*, Publications of the Scuola Normale Superiore Vol. 1 (Edizioni della Normale, Pisa, 2011), https://books.google.com/books?id=l7AIDhbWrTIC.